LA-UR- 00-3597

Title: STUDY OF RESIDUAL NUCLIDE YIELDS IN 1.0 GeV PROTON IRRADIATED 208Pb AND 2.6 GeV PROTON IRRADIATED NAT W THIN TARGETS

Author(s): Yury E. Tiarenko, Oleg Shvedov, Vyachelslav F. Batyaev, Valery M. Zhivun, Evgeny I. Karpikhin, Ruslan D. Mulambetov, Dmitry V. Fischenko, Svetlana V. Kvasova
Stepan G. Mashnik, Richard E. Prael

Submitted to: SHIELDING ASPECTS OF ACCELERATORS, TARGETS AND IRRADIATION FACILITIES (SATIF-5)
17-21 July, 2000

DISCLAIMER

STUDY OF RESIDUAL PRODUCT NUCLIDE YIELDS IN 1.0 GeV PROTON IRRADIATED ^{208}Pb AND 2.6 GeV PROTON IRRADIATED ^{NAT}W THIN TARGETS

Yury E. Titarenko, Oleg V. Shvedov, Vyacheslav F. Batyaev, Valery M. Zhivun, Evgeny I. Karpikhin, Ruslan D. Mulambetov, Dmitry V. Fischenko, Svetlana V. Kvasova
Institute for Theoretical and Experimental Physics
B. Cheremushkinskaya 25, 117259 Moscow, Russia

Stepan G. Mashnik, Richard E. Prael, Arnold J. Sierk
Los Alamos National Laboratory,Los Alamos, NM 87545, USA

Abstract

Some 113 residual product nuclide yields in a 1.0 GeV proton-irradiated thin monoisotopic ^{208}Pb sample and some 107 residual product nuclide yields in a 2.6 GeV proton-irradiated ^{nat}W sample have been measured and simulated by different codes. The irradiations were made using proton beams extracted from the ITEP synchrotron. The nuclide yields were γ-spectrometered directly using a high-resolution Ge-detector. The γ-spectra were processed by the GENIE2000 code. The ITEP-developed SIGMA code was used together with the PCNUDAT nuclear decay database to identify the γ-lines and to determine the cross-sections. The ^{27}Al(p,x)^{22}Na reaction was used to monitor the proton flux.

The measured yields are compared with their values simulated by the LAHET, CEM95, HETC, CASCADE, INUCL, YIELDX, and other codes. Estimates of the mean deviation factor are used to demonstrate the predictive power of the codes. The results obtained may be of interest in studying the parameters of the Pb and W target modules of the hybrid Accelerator-Driven System (ADS) facilities [1-3].

Introduction

At present, the Pb-Bi eutectic and W are regarded as the most promising target materials for ADS facilities [1-3]. At the same time, the high-energy irradiation mode of using the materials necessitates additional studies of the nuclear-physics characteristics of Pb, Bi, and W, particularly the yields of residual product nuclei under proton irradiation in a broad range of energies from a few MeV to 2-3 GeV. The results of the studies are extremely important when designing even demo versions of the ADS facilities.

Undoubtedly, the computational methods will play an important role when forming a set of nuclear constants for ADS facilities. Therefore, verification of the most extensively used simulation codes has proved to be of high priority.

Basic definitions and computational relations

The formalism of representing the reaction product yields (cross sections) in high-energy proton-irradiated thin targets is described in sufficient detail in [4]. In terms of the formalism, the variations in the concentration of any two chain nuclides produced in an irradiated target ($N_1 \xrightarrow{\lambda_1} N_2 \xrightarrow{\lambda_2}$) may be presented to be a set of differential equations that describe the production and decays of the nuclides. By introducing a formal representation of the time functions of the type $F_i(t) = \left(1 - e^{-\lambda_i \tau}\right) \cdot \frac{1 - e^{-\lambda_i k T}}{1 - e^{-\lambda_i T}}$ ($i = 1,2,Na$; τ is duration of accelerated proton pulse; T is pulse repetition period; k is the number of pulses within the irradiation period), which characterize the nuclide decays within the irradiation time, and by expressing (similar to the relative measurements) the proton fluence size via monitor reaction cross section σ_{St}, we can present the unknowns as

$$\sigma_1^{cum} = \frac{A_0}{\eta_1 \varepsilon_1 F_1 N_{Na}} \cdot \frac{N_{Al}}{N_T} \cdot \frac{F_{Na}}{\lambda_{Na}} \cdot \sigma_{st} \qquad (1)$$

$$\sigma_1^{cum} = \frac{A_1}{\nu_1 \eta_2 \varepsilon_2 F_1 N_{Na}} \cdot \frac{N_{Al}}{N_T} \cdot \frac{\lambda_2 - \lambda_1}{\lambda_2} \frac{F_{Na}}{\lambda_{Na}} \cdot \sigma_{st} \qquad (2)$$

$$\sigma_2^{ind} = \left(\frac{A_2}{F_2} + \frac{A_1}{F_1} \cdot \frac{\lambda_1}{\lambda_2}\right) \cdot \frac{1}{\eta_2 \varepsilon_2 N_{Na}} \cdot \frac{N_{Al}}{N_T} \cdot \frac{F_{Na}}{\lambda_{Na}} \cdot \sigma_{st} \qquad (3)$$

$$\sigma_2^{cum} = \sigma_2^{ind} + \nu_1 \cdot \sigma_1^{cum} = \left(\frac{A_1}{F_1} + \frac{A_2}{F_2}\right) \cdot \frac{1}{\eta_2 \varepsilon_2 N_{Na}} \cdot \frac{N_{Al}}{N_T} \cdot \frac{F_{Na}}{\lambda_{Na}} \cdot \sigma_{st} \qquad (4)$$

where σ_1^{cum} is the cumulative cross section of the first nuclide; σ_2^{ind} and σ_2^{cum} are the independent and cumulative cross sections of the second nuclide; N_{Al} and N_T are numbers of nuclei in monitor (standard) and in experimental sample, respectively; η_1 and η_2 are γ-line yields; ε_1 and ε_2 are the spectrometer effectiveness at energies E_1 and E_2; ν_1 is the branching ratio of the first nuclide; λ_1, λ_2, λ_{Na} are, respectively, the decay constants of the first and second nuclides and of the monitor (^{22}Na or ^{24}Na).

The factors A_0, A_1, and A_2 are calculated through fitting the measured counting rates in the total absorption peaks, which correspond to energies E_1 (the first nuclide) and E_2 (the second nuclide), by exponential functions. It should be noted that formulas (1)-(4) were deduced on assumption that the γ-intensities of two nuclides produced under irradiation are recorded up to the desired accuracy within a period from irradiation end to the moment of the ultimate detectable intensity. If, for some reasons, the factor A_1 cannot be found, then the factor A_2 will be used together with expression (14) from [4] to determine the constant (σ_2^{cum*}), which may be called the supra cumulative yield:

$$\sigma_2^{cum*} = \sigma_2 + \frac{\lambda_1}{\lambda_1 - \lambda_2} \nu_1 \cdot \sigma_1^{cum} = \cdot \frac{A_2}{N_T \Phi \eta_2 \varepsilon_2 F_2} \qquad (5)$$

The resultant value may prove to be very different from σ_2^{cum}. Nevertheless, the supra cumulative yield can be either used directly to verify the codes, or determined further up to σ_2^{cum} if the latter is obtained elsewhere (for example in the "inverse" kinematics experiments).

Experimental techniques

A 10.5-cm diameter, 139.4 mg/cm^2 monoisotopic ^{208}Pb metal foil sample (97.2%^{208}Pb, 1.93%^{207}Pb, 0.87%^{206}Pb, <0.01%^{204}Pb, <0.00105% of chemical impurities) and a 38.1 mg/cm^2 ^{nat}W

metal foil sample (99.95%W, <0.05% of chemical impurities), both of 10.5-cm diameter, were proton-irradiated. 139.6 mg/cm^2 and 139.1 mg/cm^2 Al foils of the same diameter were used as monitors Chemical impurities in the monitor did not exceed 0.001%.

The samples were irradiated by the external proton beam from the ITEP U-10 synchrotron [4]. The average flux density during irradiation of Pb and W samples was $1.4 \cdot 10^{10}$p/cm^{2}s and $2.8 \cdot 10^{10}$ p/cm^{2}s, respectively.

The measurements were supported by extra researches aimed at reducing the systematic errors in the experimental results. The researches included

- experiments to specify the neutron component in the extracted proton beams,
- experiments to specify the ^{27}Al(p,x)^{24}Na monitor reaction cross section,
- studies to specify the dependence of the γ-spectrometer detection effectiveness on the position geometry of irradiated sample,
- studies to optimize the γ-spectrum simulation codes.

Figs. 1 and 2 show the results of measuring the neutron component in the extracted proton beams. Fig. 3 presents the monitor reaction cross sections. The height-energy dependence is displayed in Fig. 4.

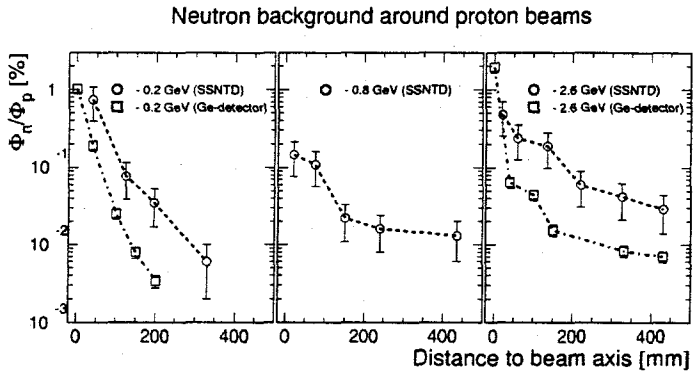

Fig. 1. The neutron background around the extracted proton beams that irradiate thin experimental samples.

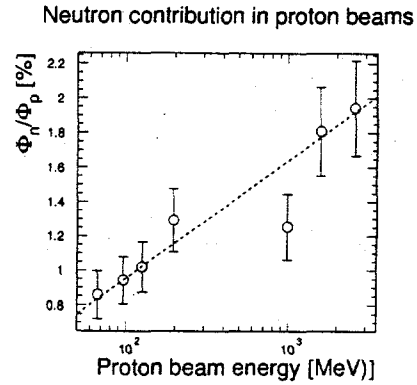

Fig. 2. Neutron component in the extracted proton beams of different energies.

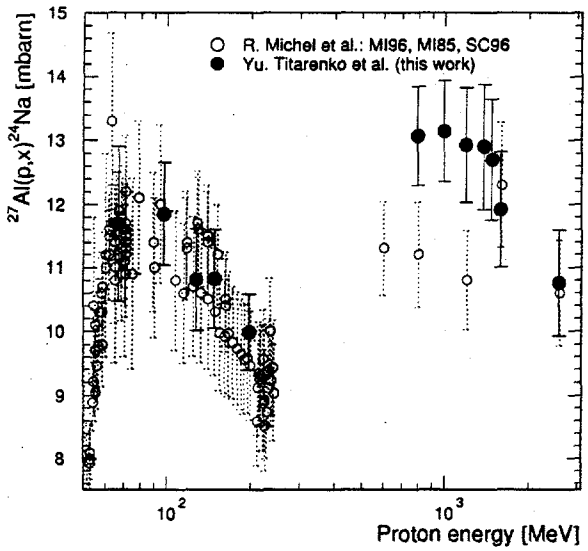

Fig. 3. The ^{27}Al(p,x)^{24}Na monitor reaction cross sections measured in this and other ([5] and references therein) works.

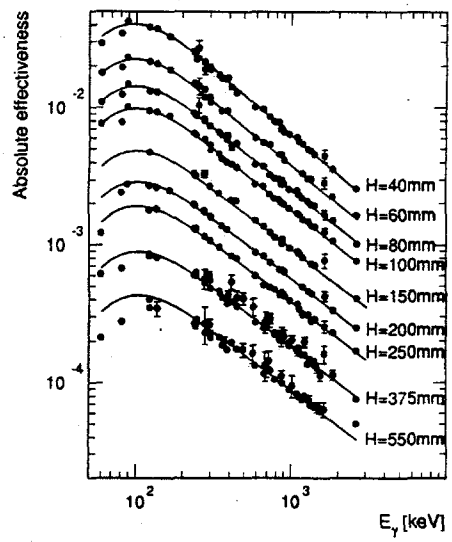

Fig. 4. The experimental and calculated detection effectivenesses of the spectrometer.

The analytical expression of the spectrometer detection effectiveness as a function of energy and sample position height is

$$\varepsilon(E,H) = \varepsilon_{base}(E) \cdot \left[\frac{(q_1 + q_2 \cdot \ln E + H_{base})}{(q_1 + q_2 \cdot \ln E + H)} \right]^2 \qquad (6),$$

where: q_1, and q_2 are the parameter defined by fitting the experimental results.

Analyzing the γ-spectrum processing codes has shown that the GENIE-2000 code is superior to the others because of its interactive mode of fitting the peaks, which permits correction of the automated computer-aided processing.

Experimental results and measurement errors

Tables 2 and 3 present the results of measuring the reaction product yields in the 1 GeV proton-irradiated ^{208}Pb and 2.6 GeV proton-irradiated ^{nat}W samples. 113 yields from ^{208}Pb have been obtained, of which 6 independent yields (i), 17 independent yields of metastable states (m), 15 independent yields of metastable and ground states (Σm_j+g), 64 cumulative yields (c), and 11 supra cumulative yields, when the addend may exceed the determination error (c*). 107 yields from ^{nat}W are presented, of which 6 independent yields (i), 9 metastable state yields (m), 5 yields of metastable and ground states (Σm_j+g), 86 cumulative yields (c), and 1 supra cumulative yield (c*).

From Tables 2 and 3 it is seen that the experimental errors are ranging within ~(6-35)%. The main contribution to the total error is from the uncertainties in the nuclear data, namely, in the absolute quantum yields and cross sections of the monitor reactions

Comparison with the experimental data obtained elsewhere

Table 1 and Fig. 9 compare some of the present results with the experimental data of other laboratories presented in [6].

Table 1. The yields (mbarn) of some products in the 1 GeV proton-irradiated ^{208}Pb inferred from the results of different laboratories

Product nuclide	ZSR Hannover	ITEP	GSI Darmstadt
^{200}Tl	22.3 ± 6.1	22.7 ± 1.5	17.0 ± 0.4(1.6)
^{196}Au	3.88 ± 0.47	4.13 ± 0.35	4.0 ± 0.1(0.4)
^{194}Au	6.85 ± 0.92	7.06 ± 0.75	6.3 ± 0.2(0.6)
^{148}Eu	0.104 ± 0.04	-	0.075 ± 0.005(0.010)
^{144}Pm	0.068 ± 0.013	-	0.036 ± 0.003(0.006)

Table 2. Experimental product nuclide yields in the 1 GeV proton-irradiated ^{208}Pb.

Product	$T_{1/2}$	Type	Yield (mbarn)
^{206}Bi	6.243d	i	4.60 ± 0.29
^{205}Bi	15.31d	i	6.20 ± 0.40
^{204}Bi	11.22h	i(m1+m2+g)	5.29 ± 0.80
^{203}Bi	11.76h	i(m+g)	4.84 ± 0.59
^{204m}Pb	67.2m	i(m)	11.0 ± 1.0
^{203}Pb	51.873h	c	31.5 ± 2.1
^{201}Pb	9.33h	c*	26.9 ± 2.4
^{200}Pb	21.5h	c	18.2 ± 1.2
^{198}Pb	2.4h	c	8.9 ± 2.1
^{197m}Pb	43.0m	c*	17.9 ± 4.0
^{202}Tl	12.23d	c	18.9 ± 1.2
^{201}Tl	72.912h	c	43.7 ± 2.9
^{200}Tl	26.1h	c	40.6 ± 2.6
^{200}Tl	26.1h	i(m+g)	22.7 ± 1.5
^{199}Tl	7.42h	c	38.5 ± 5.2
$^{198m1}Tl$	1.87h	i(m1+m2)	17.6 ± 3.6
^{198}Tl	5.30h	c	35.9 ± 5.0
^{196m}Tl	84.6m	i(m)	34.8 ± 4.4
^{203}Hg	46.612d	c	4.03 ± 0.27
^{197m}Hg	23.8h	i(m)	10.7 ± 0.7
^{195m}Hg	41.6h	i(m)	13.6 ± 2.0
^{193m}Hg	11.8h	i(m)	18.9 ± 2.5
^{192}Hg	4.85h	c	35.2 ± 2.8
^{198m}Au	54.48h	i(m)	1.01 ± 0.14
^{198}Au	64.684h	i(m+g)	2.11 ± 0.22
^{198}Au	64.684h	i	1.09 ± 0.30
^{196}Au	6.183d	i(m1+m2+g)	4.13 ± 0.35
^{195}Au	186.098d	c	48.7 ± 5.5
^{194}Au	38.020h	i(m1+m2+g)	7.06 ± 0.75
^{192}Au	4.94h	c	46.9 ± 6.6
^{192}Au	4.94h	i(m1+m2+g)	11.6 ± 1.7
^{191}Pt	69.6h	c	40.1 ± 4.4
^{189}Pt	10.87h	c	46.8 ± 4.8
^{188}Pt	10.2d	c	40.5 ± 2.9
^{190}Ir	11.78d	c	0.69 ± 0.06
^{188}Ir	41.5h	c	43.2 ± 3.2
^{188}Ir	41.5h	i(m+g)	2.93 ± 0.69
^{186}Ir	16.64h	c*	20.8 ± 1.9
^{185}Ir	14.4h	c*	34.8 ± 2.3
^{184}Ir	3.09h	c*	39.5 ± 3.0
^{185}Os	93.6d	c	41.8 ± 2.8
^{183m}Os	9.9h	i(m)	23.2 ± 1.5
^{182}Os	22.1h	c	42.0 ± 2.8
^{183}Re	70.0d	c	41.7 ± 2.9
^{182}Re	12.7h	c	45.2 ± 3.7
^{181}Re	19.9h	c	43.1 ± 5.9
^{179}Re	19.7m	c*	47.8 ± 4.2
^{177}W	2.25h	c	30.1 ± 3.5
^{176}W	2.30h	c	30.8 ± 4.3
^{176}Ta	8.09h	c	34.5 ± 3.6
^{173}Ta	3.14h	c	31.0 ± 3.9
^{172}Ta	36.8m	c*	17.3 ± 2.3
^{175}Hf	70.0d	c	31.3 ± 2.3
^{173}Hf	23.6h	c	28.4 ± 2.6
^{172}Hf	683.017d	c	24.1 ± 1.6
^{171}Hf	12.1h	c	18.2 ± 2.8
^{170}Hf	16.01h	c	22.1 ± 6.8
^{172}Lu	6.7d	c	23.9 ± 1.7
^{172}Lu	6.7d	i(m+g)	0.19 ± 0.05
^{171}Lu	8.24d	c	26.1 ± 1.8
^{170}Lu	48.288h	c	21.7 ± 2.9
^{169}Lu	34.06h	c	18.6 ± 1.2
^{169}Yb	32.026d	c	20.9 ± 1.5
^{166}Yb	56.7h	c	16.1 ± 1.1
^{167}Tm	9.25d	c	19.4 ± 4.0
^{165}Tm	30.06h	c	14.4 ± 1.4
^{160}Er	28.58h	c	8.80 ± 0.60
^{157}Dy	8.14h	c	5.73 ± 0.45
^{155}Dy	9.90h	c*	3.66 ± 0.27
^{155}Tb	5.32d	c	4.16 ± 0.39
^{153}Tb	56.16h	c*	2.52 ± 0.25
^{152}Tb	17.50h	c*	2.10 ± 0.17
^{153}Gd	241.6d	c	2.60 ± 0.23
^{149}Gd	9.28d	c	2.24 ± 0.18
^{146}Gd	48.27d	c	1.26 ± 0.09
^{147}Eu	24.0d	c	0.98 ± 0.31
^{146}Eu	4.59d	c	1.63 ± 0.11
^{146}Eu	4.59d	i	0.37 ± 0.05
^{143}Pm	265.0d	c	1.02 ± 0.13
^{139}Ce	137.64d	c	0.83 ± 0.06
^{121m}Te	154.0d	i(m)	0.44 ± 0.04
^{121}Te	16.78d	c	1.11 ± 0.11
^{119m}Te	4.7d	i(m)	0.40 ± 0.04
^{120m}Sb	5.76d	i(m)	0.54 ± 0.05
^{114m}In	49.51d	i(m1+m2)	0.95 ± 0.19
^{110m}Ag	249.79d	i(m)	1.12 ± 0.09
^{106m}Ag	8.28d	i(m)	0.89 ± 0.08
^{105}Ag	41.29d	c	0.65 ± 0.12
^{105}Rh	35.36h	c	4.63 ± 0.54
^{101m}Rh	4.34d	i(m)	1.29 ± 0.16

^{103}Ru	39.26d	c	3.84 ± 0.26
^{96}Tc	4.28d	i(m+g)	1.20 ± 0.09
^{95}Tc	20.0h	c	1.38 ± 0.13
^{96}Nb	23.35h	i	2.31 ± 0.19
^{95}Nb	34.975d	c	5.41 ± 0.34
^{95}Nb	34.975d	i(m+g)	3.03 ± 0.2
^{95}Zr	64.02d	c	2.34 ± 0.15
^{89}Zr	78.41h	c	2.30 ± 0.16
^{88}Zr	83.4d	c	0.76 ± 0.08
^{90m}Y	3.19h	i(m)	4.82 ± 0.39
^{88}Y	106.65d	c	4.03 ± 0.27
^{88}Y	106.650d	i(m+g)	3.41 ± 0.25
^{87}Y	79.8h	c*	2.94 ± 0.23
^{85}Sr	64.84d	c	2.76 ± 0.22
^{86}Rb	18.631d	i(m+g)	5.48 ± 0.66
^{83}Rb	86.2d	c	3.46 ± 0.28
^{82m}Rb	6.472h	i(m)	2.73 ± 0.30
^{82}Br	35.3h	i(m+g)	2.17 ± 0.14
^{75}Se	119.77d	c	1.34 ± 0.09
^{74}As	17.77d	i	1.86 ± 0.18
^{59}Fe	44.503d	c	0.91 ± 0.08
^{65}Zn	244.26d	c	0.79 ± 0.19
^{46}Sc	83.81d	i(m+g)	0.35 ± 0.06

Table3. Experimental product nuclide yields in the 2.6 GeV proton-irradiated ^{nat}W

Product	$T_{1/2}$	Type	Yield (mbarn)
^{177}W	2.25h	c	13.9 ± 1.9
^{176}W	2.30h	c	9.9 ± 2.9
^{184}Ta	8.7h	c	4.44 ± 0.43
^{183}Ta	5.1d	c	10.5 ± 1.0
^{182}Ta	114.43d	c	12.9 ± 1.3
^{178m}Ta	2.36h	i(m)	8.1 ± 1.3
^{176}Ta	8.09h	c	29.3 ± 3.3
^{175}Ta	10.5h	c	26.0 ± 2.8
^{174}Ta	63m	c	25.8 ± 2.8
^{181}Hf	42.39	c	1.26 ± 0.12
^{173}Hf	23.6h	c	29.9 ± 2.5
^{171}Hf	12.1h	c	19.6 ± 2.4
^{170}Hf	16.01h	c	19.6 ± 4.0
^{172}Lu	6.7d	i(m+g)	4.32 ± 0.56
^{171}Lu	8.24d	c	30.1 ± 2.46
^{171}Lu	8.24d	i(m+g)	10.8 ± 2.0
^{170}Lu	48.288h	c	24.8 ± 2.2
^{169}Lu	34.06h	c	22.2 ± 1.8
^{167}Lu	51.5m	c	23.4 ± 2.4
^{167}Yb	17.5m	c	24.9 ± 2.8
^{166}Yb	56.7h	c	24.6 ± 2.1
^{166}Tm	7.7h	c	27.2 ± 2.3
^{166}Tm	7.7h	i	2.36 ± 0.46
^{165}Tm	30.06h	c	27.1 ± 2.4
^{163}Tm	1.81h	c	26.3 ± 3.3
^{161}Tm	33m	c	21.0 ± 2.5
^{161}Er	3.21h	c	24.3 ± 2.5
^{160}Er	28.58h	c	23.9 ± 2.2
^{157}Er	25m	c	26.4 ± 5.9
^{156}Er	19.5m	c	15.9 ± 2.4
^{160m1}Ho	5.02h	i(m_1+m_2)	24.9 ± 2.3
^{157}Ho	12.6m	c	26.1 ± 6.8
^{156}Ho	56m	c	19.6 ± 1.8
^{157}Dy	8.14h	c	24.2 ± 2.2
^{155}Dy	9.90h	c	22.1 ± 1.9
^{153}Dy	6.4h	c	14.0 ± 1.9
^{152}Dy	2.38h	c	15.6 ± 1.3
^{155}Tb	5.32d	c	22.7 ± 1.9
^{153}Tb	56.16h	c	18.9 ± 1.7
^{152}Tb	17.50h	c	16.2 ± 1.3
^{151}Tb	17.609h	c	16.7 ± 1.4
^{149}Tb	4.118h	c	6.85 ± 0.62
^{147}Tb	1.70h	c	2.15 ± 0.34
^{151}Gd	124.0d	c	19.0 ± 2.2
^{149}Gd	9.28d	c	20.4 ± 1.7
^{147}Gd	38.1h	c	18.6 ± 1.6
^{146}Gd	48.27d	c	19.4 ± 1.6
^{145}Gd	23.0m	c	12.9 ± 1.4
^{149}Eu	93.1d	c	26.7 ± 3.4
^{147}Eu	24.0d	c	22.4 ± 2.0
^{146}Eu	4.59d	c	23.0 ± 1.9
^{146}Eu	4.59d	i	3.62 ± 0.31
^{145}Eu	5.93d	c	17.8 ± 1.6
^{139}Nd	5.5h	c	2.87 ± 0.43
^{139}Ce	137.64d	c	19.8 ± 1.6
^{135}Ce	17.7h	c	17.8 ± 1.5
^{132}Ce	3.51h	c	16.3 ± 2.7
^{132}La	4.8h	c	14.5 ± 1.6
^{131}Ba	11.50d	c	16.2 ± 1.3
^{126}Ba	100m	c	7.9 ± 1.1
^{129}Cs	32.06h	c	18.7 ± 1.6
^{127}Xe	36.4d	c	15.4 ± 1.3

^{125}Xe	16.9h	c	14.2 ± 1.2	^{89}Zr	78.41h	c	3.46 ± 0.28
^{123}Xe	2.08h	c	15.6 ± 1.3	^{88}Zr	83.4d	c	2.56 ± 0.27
^{122}Xe	20.1h	c	11.7 ± 1.0	^{88}Y	106.65d	c	3.49 ± 0.34
^{121}Te	16.78d	c	10.7 ± 1.1	^{88}Y	106.65d	i(m+g)	1.56 ± 0.22
^{119}Te	16.03h	c	9.17 ± 0.74	^{87}Y	79.8h	c	4.13 ± 0.34
^{119m}Te	4.7d	i(m)	1.97 ± 0.17	^{83}Sr	32.41h	c	1.96 ± 0.93
^{117}Te	62m	c	8.81 ± 0.77	^{84}Rb	32.77d	i (m+g)	1.31 ± 0.14
^{118m}Sb	5.0h	i(m)	1.08 ± 0.22	^{83}Rb	86.2d	c	3.34 ± 0.58
^{115}Sb	32.1m	c*	9.85 ± 0.88	^{82m}Rb	6.472h	i(m)	1.89 ± 0.17
^{113}Sn	115.09d	c	7.55 ± 0.67	^{77}Kr	74.4m	c	1.71 ± 0.18
^{111}In	2.8049d	c	7.44 ± 0.74	^{75}Se	119.77d	c	2.38 ± 0.22
^{110m}In	4.9h	i(m)	3.29 ± 0.29	^{73}Se	7.15h	c	1.03 ± 0.11
^{109}In	4.2h	c	5.12 ± 0.43	^{74}As	17.77d	c	1.38 ± 0.16
^{106m}Ag	8.28d	i(m)	1.70 ± 0.16	^{69m}Zn	13.76h	i(m)	0.420 ± 0.038
^{105}Ag	41.29d	c	5.33 ± 0.69	^{54}Mn	312.12d	i	2.51 ± 0.42
^{100}Pd	87.12h	c	1.24 ± 0.27	^{51}Cr	27.704d	c	4.5 ± 1.4
^{100}Rh	20.8h	c	3.97 ± 0.44	^{48}V	15.973d	c	0.557 ± 0.062
^{100}Rh	20.8h	i	2.68 ± 0.28	^{48}Sc	43.67h	i	0.668 ± 0.091
^{99m}Rh	4.7h	c	2.41 ± 0.28	^{43}K	22.3h	c	0.681 ± 0.084
^{97}Ru	69.6h	c	3.13 ± 0.28	^{28}Mg	20.91h	c	0.910 ± 0.089
^{96}Tc	4.28d	i(m+g)	1.73 ± 0.20	^{24}Na	14.959h	c	4.09 ± 0.34
^{93m}Mo	6.85h	i(m)	1.61 ± 0.13	^{7}Be	53.29d	i	8.7 ± 1.0
^{90}Nb	14.6h	c	2.58 ± 0.22				

5. Simulation of experimental results

Simulation techniques are of essential importance when forming the set of nuclear constants to be used in designing the ADS facilities because they are universal and save much time and labour. At the same time, the present-day accuracy and reliability of the simulated data are inferior to experiment. Besides, the simulation codes are of different abilities to work when used to study the reactions that are of practical importance.

Considering the above, the present work is primarily aimed at verifying the simulation codes used most extensively for the above purpose with a view to not only estimating their ability to work when applied to the issues discussed here, but also opening up the ways to update them.

The following seven simulation codes were examined to meet these requirements:

- the CEM95 cascade-exciton code [7],
- the CASCADE cascade-evaporation-fission-transport code [8],
- the INUCL cascade-pre equilibrium-evaporation-fission code [9],
- the LAHET cascade-evaporation-fission code [10],
- the YIELDX semi-phenomenological code [11],
- the CASCADE/INPE cascade-evaporation-fission-transport code [12]
- the CEM2k cascade-exciton code [16], modification of CEM95 code,

Contrary to the simulation results, the experimental data include not only independent, but also (and mainly) cumulative and supra cumulative, residual product nuclei. To get a correct comparison between the experimental and simulation data, therefore, the cumulative yields must be simulated on the basis of the simulated independent yields.

Since any branched isobaric chain can be presented to be a superposition of a few linear chains, the simulated cumulative and supra cumulative yields of the n-th nuclide can be calculated as

$$\sigma_n^{cum} = \sigma_n^{ind} + \sum_{i=1}^{n-1} \sigma_i^{ind} \prod_{j=i}^{n-1} \nu_j , \qquad (6)$$

$$\sigma_n^{cum^*} = \sigma_n^{ind} + \frac{\lambda_{n-1}}{\lambda_{n-1} - \lambda_n} \nu_{n-1} \cdot \left[\sigma_{n-1}^{ind} + \sum_{i=1}^{n-2} \left(\sigma_i^{ind} \prod_{j=i}^{n-2} \nu_j \right) \right] \qquad (7)$$

The branching ratios of the decay chains were retrieved from [13].

To get a correct comparison among the simulation results obtained by different codes, the results were renormalized to unified cross sections for proton-target nucleus inelastic interactions [14].

If an experiment-simulation difference of not above 30% ($0.77<\sigma_{calc.}/\sigma_{exp.}<1.3$) [15] is taken to be the coincidence criterion, the simulation accuracy can be presented to be the ratio of the number of the coincidences to the number of the comparison events. The 30% level meets the accuracy requirements of the cross sections for nuclide production to be used in designing the ADS plants [15]. The mean simulated-to-experimental data ratio can be used as another coincidence criterion:

$$\langle F \rangle = 10^{\sqrt{\langle (\lg(\sigma_{cal,i}/\sigma_{exp,i})^2 \rangle}} \qquad (8)$$

with its standard deviation

$$S(\langle F \rangle) = \left\langle \left[\lg\left(\sigma_{calc,i}/\sigma_{exp,i}\right) - \lg\left(\langle F \rangle\right) \right]^2 \right\rangle \qquad (9)$$

where $\langle\ \rangle$ designates averaging over all i = 1...N_S (here, N_S is the number of the experimental and simulated results used in the comparisons).

The mean ratio <F> together with its standard deviation S(<F>) defines the interval [⟨F⟩/S(⟨F⟩) : ⟨F⟩xS(⟨F⟩)] that covers about 2/3 of the simulation-to-experiment ratios.

The two criteria are considered sufficient for any conclusion concerning the ability of the simulation codes to work to be derived.

The default options were committed to practical usage of the simulation codes.

Comparison of experiment with simulation

The results obtained with the above codes are presented in:

- Figs. 5 and 6 that show the results of detailed comparison between the simulated and experimental data on the radioactive reaction product yields,
- Figs. 7 and 8 that show the simulated mass distributions of the reaction products together with the measured cumulative (and supra cumulative) yields of the products that are at the immediate proimity to the stable isobar of the given mass (the sum of such yields from either sides in case both left- and right-hand branches of the chain are present). Obviously, the displayed simulation results do not contradict the experimental data if the simulated values run above the experimental data and follow the general trend of the latter. This is because the direct □-spectroscopy identifies only those radioactive products that, as a rule, include a significant fraction of the total mass yield, but, should a stable isobar of the given mass be present, are never equal to the total mass yield;
- In Fig. 9 that shows the experimental and simulated independent yields of reaction products in the form of isotopic mass distributions for some elements.

Table 4 presents the statistics of the comparison between the experimental and simulated reaction product yields in the thin ^{208}Pb and ^{nat}W samples irradiated by 1.0 GeV and 2.6 GeV protons, respectively.

Table 4. Comparison statistics for ^{208}Pb and $^{nat.}W$

Code	Pb, E_p=1.0GeV N_T = 113, N_G = 90			W, E_p=2.6GeV N_T = 107, N_G = 96		
	$N_{C1.3}/N_{C2.0}/N_S$	⟨F⟩	S(⟨F⟩)	$N_{C1.3}/N_{C2.0}/N_S$	⟨F⟩	S(⟨F⟩)
LAHET	41/65/90	2.06	1.78	11/50/93	2.89	2.04
CEM95	-	-	-	26/62/84	2.94	2.47
CEM2k	38/58/66	1.62	1.44	-	-	-
CASCADE	33/60/86	2.28	1.90	45/68/94	2.84	2.50
CASCADE/INPE	36/66/84	1.84	1.56	-	-	-
INUCL	29/54/90	2.87	2.16	34/54/86	4.20	3.31
YIELDX	30/54/90	2.87	2.24	25/57/96	2.36	1.81

Table 3 presents the total number of measured yields, N_T; the number of the measured yields selected to compare with simulated data, N_G; the number of the product nuclei whose yields were simulated by a particular code, N_S; the number of the comparison events when the simulated data differ from the experimental results by not above 30%, $N_{C1.3}$; the number of the comparison events when the simulated data differ from the experimental results by not more than a factor of 2.0, $N_{C2.0}$.

Since ~30% of all secondary nuclei are not the spallation reaction products, the quality criterion of the codes is their ability to simulate the high-energy fission and fragmentation processes.

The following conclusions follow from the analysis of the experiment-simulation comparison results presented in Table 1 and in Figs. 5-9:

1. Generally, all codes can quite adequately simulate the weak spallation reactions (the A◊180 products for ^{208}Pb and the A◊150 products for ^{nat}W), with the simulation results differing from experimental data within a factor of 2.
2. In the deep spallation range (150<A<180 for ^{208}Pb and 110<A<150 for ^{nat}W) the simulation codes are of very different predictive powers, namely,
   - the LAHET, CEM2k, CASCADE/INPE, and YIELDX predictions are actually the same as the experimental data;
   - the CASCADE code simulates the A>160 product yields adequately. Below A = 160, however, the simulated data get underestimated progressively (up to a factor of 5) compared with experiment;
   - the INUCL code underestimates the yields of all the products by a factor of 2-10 in all the above mass ranges.
3. In the mass range characteristic of the fission products (50<A<150 for ^{208}Pb and 30<A<110 for ^{nat}W), the INUCL code predictions are in the best agreement with experiment when describing the the yields from ^{208}Pb. As a rule, the INUCL-simulated data differ from experiment by not above a factor of 1.5. In the case of ^{nat}W, however, the prediction quality deteriorates substantially. The LAHET-simulated yields in the same mass range are underestimated by a factor of 1.5-10.0. The YIELDX-simulated yields are both under- and over-estimated by a factor of up to 30 without showing any physical regularities. The CASCADE/INPE-simulated yields of the 130<A<150 reaction products are much underestimated (by 1-2 orders), while the simulated 40<A<130 product yields agree with experiment to within, as a rule, a factor of 2. Generally, all the codes exhibit the feature noted above for INUCL, namely, the yield prediction quality in the case of ^{nat}W is much worse compared with ^{208}Pb because, probably, the fission cross sections of the compound nuclei with explicitly low fissility are difficult to calculate.

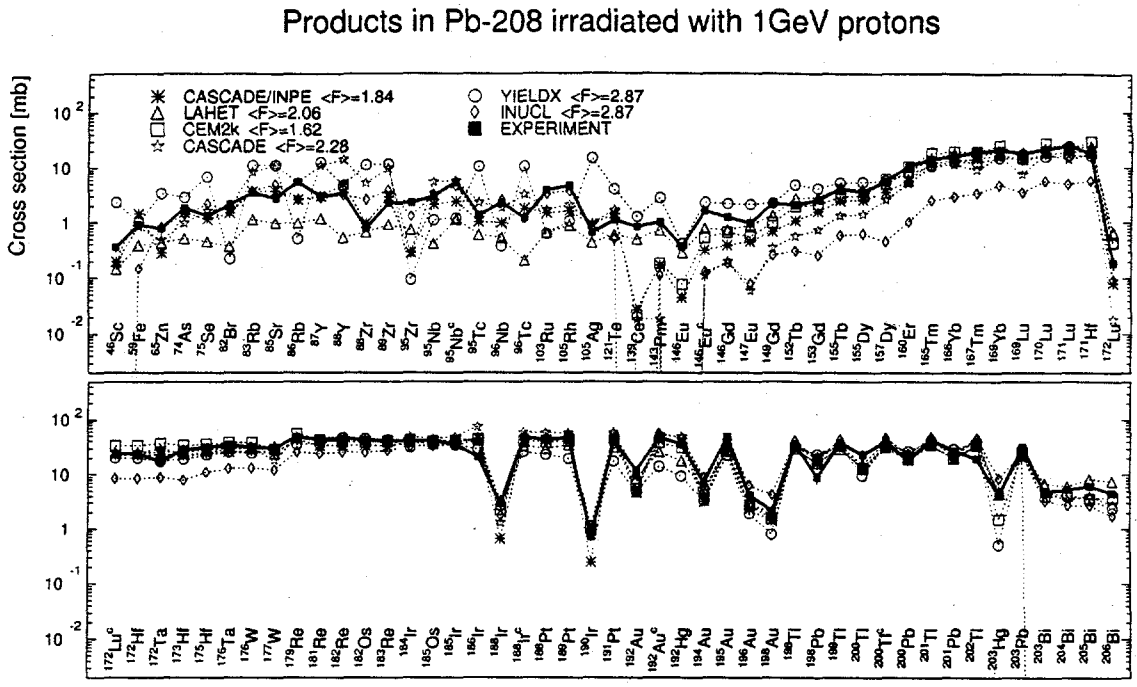

Fig.5. Product comparison between the experimental (closed symbols) and simulated (open symbols) yields of radioactive reaction products from ^{208}Pb irradiated with 1 GeV protons. The cumulative yields are labeled "c" when respective independent yields are also shown.

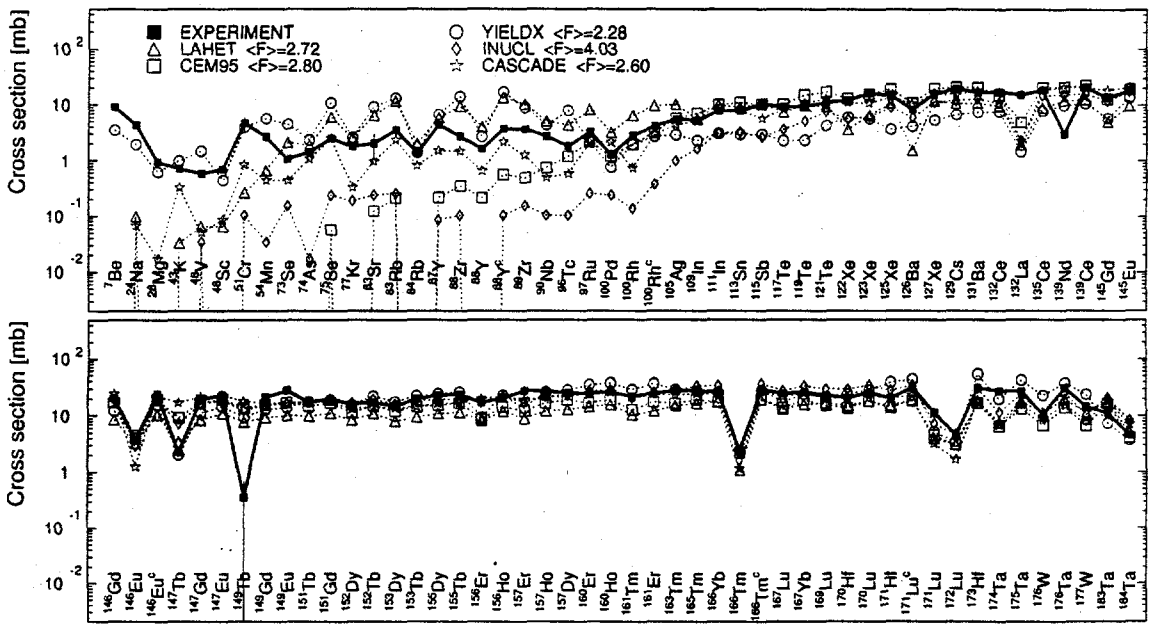

Fig.6. Product comparison between the experimental (closed symbols) and simulated (open symbols) yields of radioactive reaction products from ^{nat}W irradiated with 2.6 GeV protons. The cumulative yields are labeled "c" when respective independent yields are also shown.

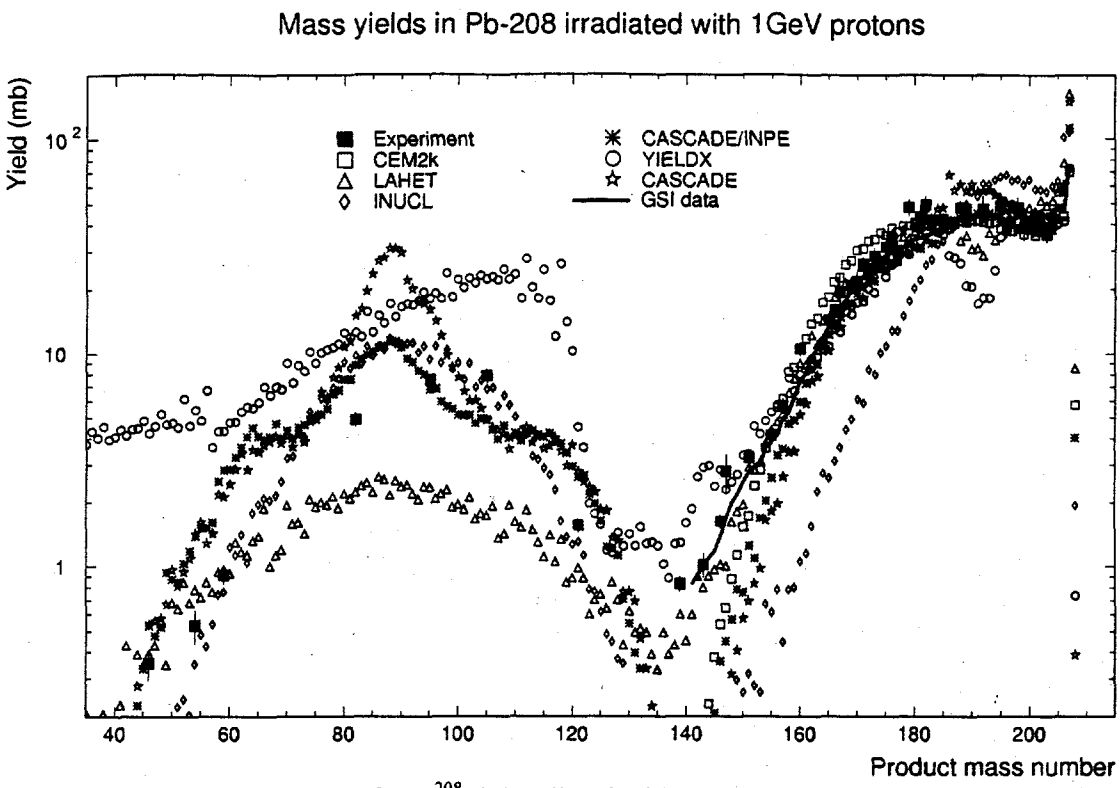

Fig. 7. Mass product yields from ^{208}Pb irradiated with 1.0GeV protons measured and calculated via the codes. The GSI data from [6] are shown too.

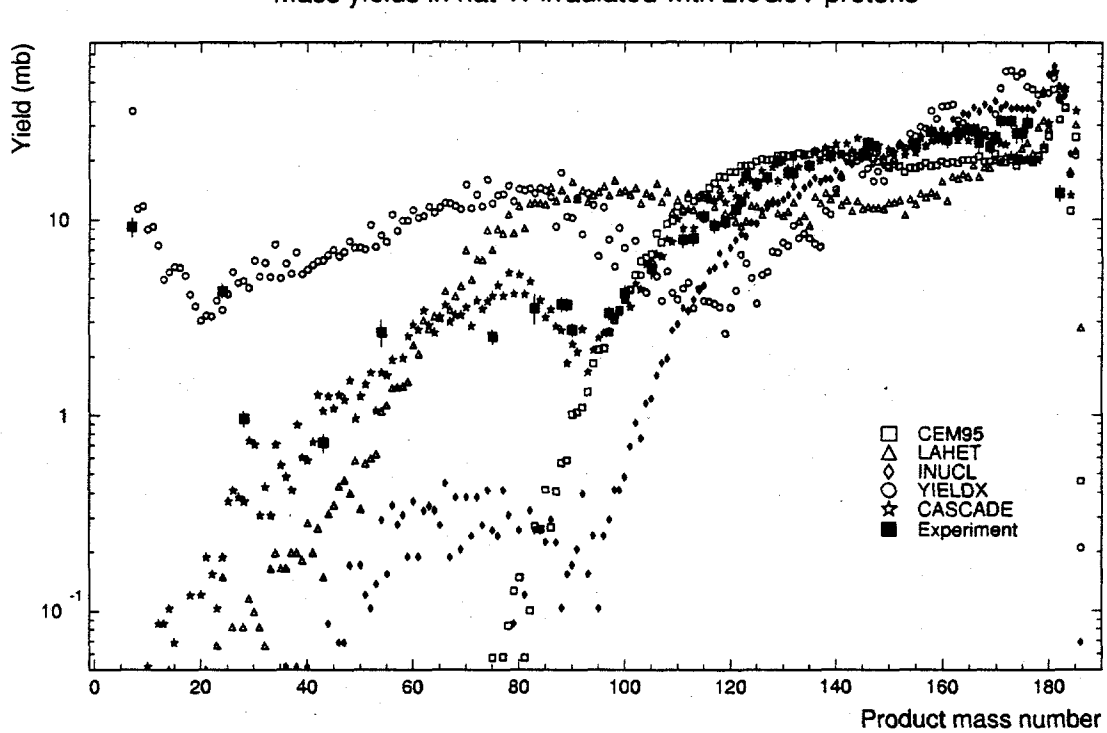

Fig. 8. Mass product yields from ^{nat}W irradiated with 2.6GeV protons measured and calculated via the codes.

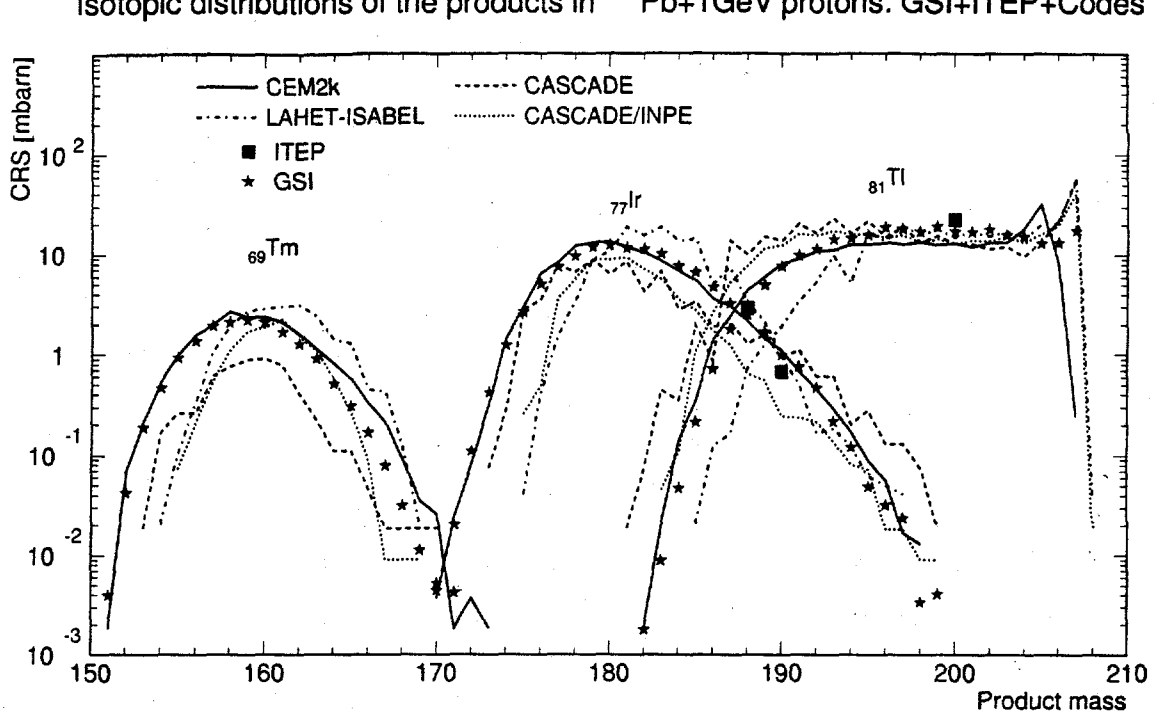

Fig. 9. Isotopic mass distributions of the reaction products in ^{208}Pb. The GSI data from [6] are shown too.

Conclusion

The trends shown by the advances of the nuclear transmutation of radioactive wastes permit us to expect that the accumulation and analysis study of nuclear data for ADS facilities will have the same rise of academic interest and practical commitments as in the nuclear reactor data during the last five decades. Therefore, the experimental data on the yields of the proton-induced reaction products as applied to the ADS main target and structure materials are urgent to accumulate. It should be emphasized also that the charge distributions in the isobaric decay chains are important to study. The information thus obtained would make it possible, first, to raise the information content of the comparisons between the experimental and simulated data and, second, to lift the uncertainties in experimental determination of the cumulative yields by establishing unambiguous relations between σ^{cum} and σ^{cum^*} for many of the reaction product masses.

Acknowledgement

The authors are grateful to Prof. Vladimir Artissiuk (Tokyo Institute of Technology) for consulting and discussion of results of simulation-to-experimental comparisons.

The work was performed under the ISTC Project #839 and was partially supported by the U. S. Department of Energy.

References

[1] Gregory J. Van Tuyle, ATW Technology Development & Demonstration Plan, LANL Report LA-UR-99-1061; Gregory J. Van Tuyle, ATW Technology & Scenarios, LANL Report LA-UR 99-771.

[2] T. Mukayama, OMEGA Program in Japan and ADS Development at JAERI, Proceedings of the Third International Conference on Accelerator-Driven Transmutation Technologies and Applications ADTT'99, Praha, June 1999. Mo-I-5.

[3] M. Salvatores, Strategies for the back-and of the fuel cycle: A scientific point of view, Proceedings of the Third International Conference on Accelerator-Driven Transmutation Technologies and Applications ADTT'99, Praha, June 1999Mo-I-4

[4] Yu. E. Titarenko, O. V. Shvedov, M. M. Igumnov, S. G. Mashnik, E. I. Karpikhin, V.D. Kazaritsky, V. F. Batyaev, A. B. Koldobsky, V. M. Zhivun, A.N. Sosnin, R. E. Prael, M. B. Chadwick, T. A. Gabriel, M. Blann, "Exerimental and theoretical Study of the Yields of Radionuclides Produced in ^{209}Bi thin target Irradiated by 1500 MeV and 130MeV Protons", Nucl. Instr. and Meth. A414 (1998)73-99.

[5] M. Gloris, R. Michel, U. Herpers, F. Sudbrok, D. Filges, "Production of residual nuclei from irradiation of thin Pb-targets with protons up to 1.6 GeV", NIM B 113 (1996) 429-433; R.Michel, M.Gloris, H.-J.Lange, I.Leya, M.Luepke, U.Herpers, B.Dittrich-Hannen, R.Roesel, Th.Schiekel, D.Filges, P.Dragovitsch, M.Suter, H.-J.Hofmann,W.Woelfli, P.W.Kubik, H.Baur, R.Wieler, "Nuclide production by proton-induced reactions on elements ($6 \leq Z \leq 29$) in the energy range from 800 to 2600 MeV", Nucl. Instr. Meth. B 103 (1995), 183-222.

[6].W. Wlazlo, T. Enqvist, P. Armbruster et. al. "Cross-sections of spallation residues produced in 1 A GeV ^{208}Pb on proton reactions" DAPNIA/SPHN-00-10 02/2000,p.1-4. (Also submitted to Phys. Rev. Lett.)

[7] K.K. Gudima, S.G. Mashnik, V.D. Toneev, Nucl. Phys. A 401 (1983) 329--361; S.G. Mashnik, User Manual for the Code CEM95, JINR, Dubna, 1995; OECD Nuclear Energy Agency Data Bank, Paris, France, 1995; http://www.nea.fr/abs/html/iaea1247.html; RSIC-PSR-357, Oak Ridge, 1995.

[8] V.S. Barashenkov, Le Van Ngok, L.G. Levchuk, Zh.Zh. Musul'manbekov, A.N. Sosnin, V.D. Toneev, S.Yu. Shmakov, JINR Report R2-85-173, Dubna, 1985; V.S. Barashenkov, F.G. Zheregi, Zh.Zh. Musul'manbekov, Yad. Fiz. 39 (1984) 1133 [Sov. J. Nucl. Phys. 39 (1984) 715]; V.S. Barashenkov, B.F. Kostenko, A.M. Zadorogny, Nucl. Phys. A 338 (1980) 413.

[9] G.A. Lobov, N.V. Stepanov, A.A. Sibirtsev, Yu.V. Trebukhovskii, ITEP Preprint ITEP-91, Moscow, 1983; A.A. Sibirtsev, N.V. Stepanov, Yu.V. Trebukhovskii, ITEP Preprint ITEP-129, Moscow, 1985; N.V. Stepanov, ITEP Preprint ITEP-81, Moscow, 1987; N.V. Stepanov, ITEP Preprint ITEP-55-88, Moscow, 1988 (in Russian).

[10] R.E. Prael, H. Lichtenstein, Los Alamos National Laboratory Report LA-UR-89-3014 (1989); see also the Web page at: http://www-xdiv.lanl.gov/XTM/lcs/lahet-doc.html.

[11] C.H. Tsao, Private communication, R. Silberberg, C.H. Tsao, Astrophys. J. 220 (1973) 315; ibid 335.

[12] Yu. A. Korovin, et al.: "Study of Accelerator-Driven Reactor systems", Kerntechnik, v.64 p.284 (1999)

[13] N.G.Gusev, P.P.Dmitriev. Radioactive Chains: Handbook, Energoatomizdat, Moscow, 1988.

[14] J.R. Letaw et al. Ap. J. Suppl., 51 (1983) 271.

[15] A. Koning, Nuclear Data Evaluation for Accelerator-Driven Systems, Second International Conference on Accelerator-Driven Transmutation Technologies and Applications. June 3-7, 1996, Kalmar, Sweeden, p.p. 438-447.

[16] S.G. Mashnik, L. Waters, and T. Gabriel, Models and codes for intermediate energy nuclear reactions (an overview). Models and Codes for Spallation Neutron Source, Special session within the SARE-5/SATIF-5 Meeting, July 17-18, 2000, Paris, France.